A high precision CMOS weak current readout circuit*

Wu Qisong(吴其松)[1,2], Yang Haigang(杨海钢)[1,†], Yin Tao(尹韬)[1], and Zhang Chong(张翀)[1,2]

(1 Institute of Electronics, Chinese Academy of Sciences, Beijing 100190, China)

(2 Graduate University of the Chinese Academy of Sciences, Beijing 100049, China)

Abstract: This paper presents a high precision CMOS weak current readout circuit. This circuit is capable of converting a weak current into a frequency signal for amperometric measurements with high precision and further delivering a 10-bit digital output. A fast stabilization-enhanced potentiostat has been proposed in the design, which is used to maintain a constant bias potential for amperometric biochemical sensors. A technique based on source voltage shifting that reduces the leakage current of the MOS transistor to the reverse diode leakage level at room temperature was employed in the circuit. The chip was fabricated in the 0.35 μm chartered CMOS process, with a single 3.3 V power supply. The interface circuit maintains a dynamic range of more than 100 dB. Currents from 1 pA to 300 nA can be detected with a maximum nonlinearity of 0.3% over the full scale.

Key words: amperometric sensor; current readout; high precision; potentiostat

DOI: 10.1088/1674-4926/30/7/075001 **EEACC:** 2570

1. Introduction

Biochemical technology together with the nanoelectronics industries has emerged as one of the most promising developments in the 21st century[1]. Biochemical sensors in particular have received a great deal of attention due to their possible applications in biomedical fields, such as in life research on the molecular level. Electrochemical biosensors, which give the detected signals or data in terms of potential or current, have been widely used in many ways, such as DNA identification[2], protein classification, neural recording, glucose determination[3,4], pH variation detection, and drug determination[5]. Electrochemical biosensors are much more economical and convenient than high performance yet bulky equipment, because they do not require expensive setups, such as electrochemical analyzers or phase-locked amplifiers, and they can be realized on a miniaturized biosensor chip[6]. Most amperometric biosensors utilize micro-electrodes or micro-arrays to detect analytes, and the output signal of most micro-electrodes is an ultra low current. So an ultra low current readout circuit for these electrodes or arrays is needed to determine the concentration of the analytes or detect and distinguish biological molecules.

Generally, the currents passing through those electrodes are very weak (10^{-12}–10^{-7}A), which brings about a great challenge for the interface circuit design. Previously, some designs have been proposed for amperometric sensors[7–11]. Each of them amplifies the small sensor current to the μA range and then measures it. In this paper, we propose a current readout circuit, which directly converts sensor redox currents into frequency signals and further delivers a 10-bit digital output, so that complicated designs of the current amplifier and the successive A/D converter are avoided. Also a wide dynamic range and low power design is easily implemented. Noting that the potentials on the sensor electrodes are quite vulnerable to cross talk signals from the following current-to-frequency converter, we develop a fast stabilization-enhanced potentiostat which makes the redox current of amperometric sensor more stable. Moreover, the circuit reduces the leakage current to a much lower level by shifting the source voltages, so that a high resolution and a wide dynamic range are guaranteed. This prototype chip was tested with a specially designed precision current source.

2. Amperometric sensors

Microelectrodes are key devices in amperometric sensors. Amperometric sensors typically consist of three electrodes: the working electrode (WE), the reference electrode (RE) and the counter or auxiliary electrode (CE)[12]. In addition, many amperometric sensors only have two electrodes (WE and CE). The readout circuit presented in this paper is designed for a two-electrode amperometric immunosensor, whose structure is shown in Fig. 1[13]. The sensor is associated with the simplified manufacturing process and has

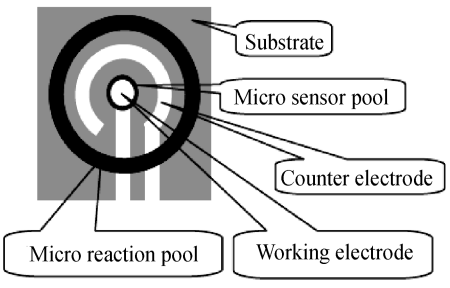

Fig. 1. Microelectrodes of the amperometric immunosensor.

* Project supported by the National High-Tech Research and Development Program of China (No. 2007AA04Z349).

† Corresponding author. Email: yanghg@mail.ie.ac.cn

Received 30 December 2008, revised manuscript received 12 March 2009

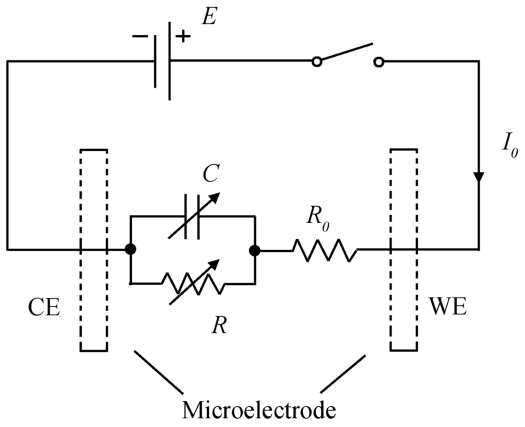

Fig. 2. Circuit model of the immunosensor.

advantages with regard to signal-to-noise ratio (SNR), response time, portability and low power[6]. To determine the concentration of an analyte, a constant potential must be applied to the sensor between the WE and the CE, such that

$$V_{\text{cell}} = V_{\text{WE}} - V_{\text{CE}}. \quad (1)$$

When V_{cell} reaches an analyte's redox potential, a redox current I_{S} that is proportional to the analyte's concentration is generated at the WE. The redox current also changes when the potential applied to the sensor changes, so that a potentiostat is needed in the readout circuit. The equivalent electrical circuit of an amperometric immunosensor is shown in Fig. 2[6], which was used as the sensor model during the system simulation and the circuit design. The redox potential of the amperometric immunosensor is between 0.3 and 0.6 V, and the redox current generally ranges from 1 pA to 200 nA.

3. Circuit description

Measuring ultra low currents off-chip is a challenging task, which requires expensive instrumentation and very careful wiring to avoid undesired parasitic leakage. To avoid these problems we have developed this on-chip readout circuit. As shown in Fig. 3, the weak current readout circuit is composed of a potentiostat, a low current controlled sawtooth oscillator, and a digital frequency meter. The potentiostat has been used to provide a constant voltage for the sensor, which generates a stable redox current that is proportional to the concentration of the electrolyte. By converting the weak current into a periodic pulse through charging and discharging the capacitor C_0, the sawtooth oscillator converts the analog signal into a digital signal, which can be processed by the successive digital circuit easily. The digital frequency meter detects the frequency of the periodic pulse, and outputs 10-bit binary code. Then we can figure out the redox current from the 10-bit binary code through a simple calibration and calculation.

3.1. Potentiostat

The main function of the potentiostat is to provide the required constant bias potential between the WE and CE in the electrochemical cell, and to make a nonperturbing measurement of the redox current. The potentiostat shown in Fig. 4 is a traditional amperometric potentiostat[6, 14–18]. The potentiostat is composed of a high gain cascoded operational transconductance amplifier (OTA) and an NMOS transistor N1. The OTA and N1 form a negative feedback loop, which forces the voltage of V_- to equal the voltage of V_+. The bias power source (V_{bias}) is used for providing a constant bias for the sensor.

Note that in the proposed current-to-frequency converter topology, the potential on the WE and the redox current are quite vulnerable to disturbance. Although the design shown in Fig. 4 provides a high impedance at the terminal Z, because of the parasitic effects of the transistor N1 and the strong periodic potential signal at the terminal Z, the redox current and the potential on the WE will be seriously disturbed in the conventional potentiostat. This condition worsens as the redox current becomes smaller. As a result, the measurement resolution is seriously reduced.

In order to provide a much more stable potential for the sensor and keep the redox current more stable, we have developed the fast stabilization-enhanced potentiostat shown in Fig. 3. A 5-pF capacitor C_3 has been used to stabilize the potential at V_-. However, if we directly connect C_3 to V_-, it will take a long time to charge C_3 to the voltage at V_+ with a small current through N1; so we use a two-direction switch to avoid this problem. Firstly, reset is set to low, K0 switches to K2, and C_3 is quickly charged to V_+ by the power source V_{bias}. Then reset resumes to high, K0 switches to K1, C_3 is connected to V_-, and the system starts to work. This fast stabilization-enhanced potentiostat makes V_- and I_{S} more stable, moreover, it does not need a long time for the system to work normally. A simulation comparison between the traditional potentiostat and the fast stabilization potentiostat is shown in Fig. 5.

The OTA used in this design is a standard folded-cascode OTA with a single-ended output[19]. For the detection of ultra low currents through the electrolyte, the input referred noise of the OTA is designed to be very low. All the transistors in the OTA design have been properly sized to minimize the equivalent input noise. The topology of the OTA is shown in Fig. 6, and the specifications of the OTA are summarized in Table 1.

3.2. Low current sawtooth oscillator

We have developed this on-chip sawtooth oscillator to convert the current signal into a periodic signal. The frequency of the periodic signal is proportional to the redox current I_{S}. The circuit topology is included in Fig. 3. The sawtooth oscillator works as follows: C_0 is firstly charged to V_{TOP} through P1 when the reset is coming. Then C_0 is steadily discharged by I_{S}, and V_{Z} decreases linearly. As soon as V_{Z} is lower than V_{REF}, V_{C} goes from high to low, and C_0 is recharged to V_{TOP} quickly. This circuit will repeat the discharging and recharging operation until the next reset signal comes. Due to the discharging and recharging operation, a sawtooth wave is generated at the terminal Z, and a periodic pulse with the same frequency as the sawtooth wave is generated at the terminal C. The periodic pulse can be easily processed by a successive digital circuit. Because C_0 is charged to V_{TOP} for an instant, the charging time

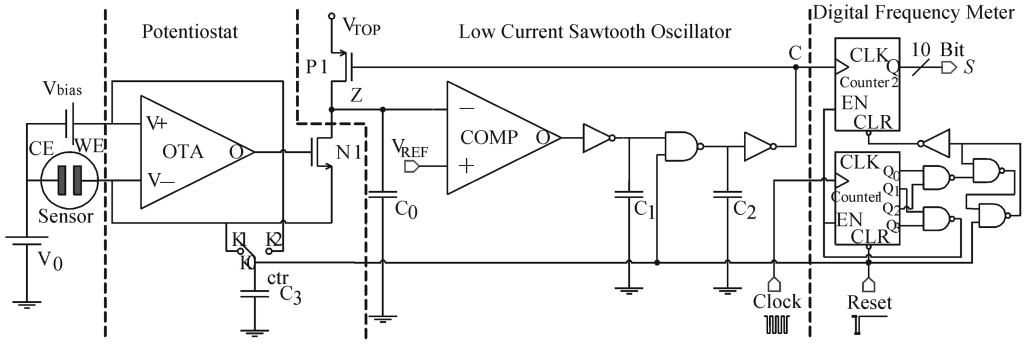

Fig. 3. Diagram of the readout circuit and the sensor system.

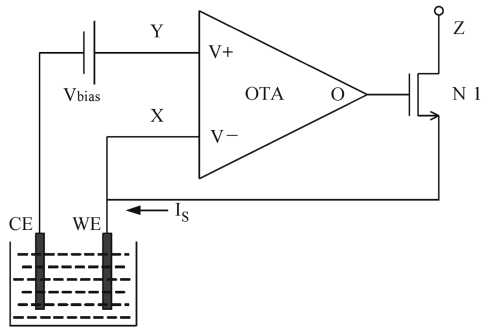

Fig. 4. Conventional potentiostat block diagram.

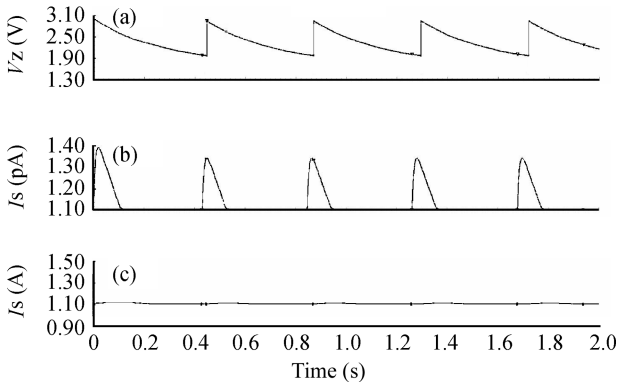

Fig. 5. Variation of I_S due to fluctuations at terminal Z: (a) Waveform at terminal Z: (b) I_S in the conventional potentiostat: (c) I_S in the fast stabilization potentiostat.

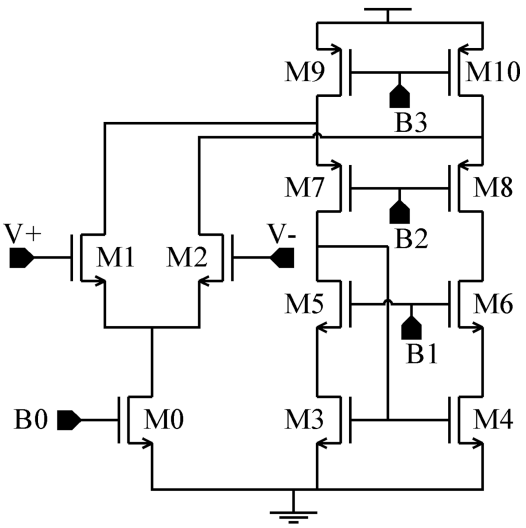

Fig. 6. Scheme of the OTA.

Table 1. Summary of the specifications of the OTA.

Parameter	Specification
Supply voltage	3.3 V
Av	75.82 dB
Phase margin	70°
GBW C_L = 2 pF	42 MHz
Output swing	1.6–2.9 V
CMRR	122.5 dB
PSRR	97.3 dB
ICMR	1.3–3.3 V
Slew rate	27.6/–26.2 V/μs

can be neglected. The period of the sawtooth wave is given by

$$T = \frac{C_0 \Delta V}{I_S}, \tag{2}$$

$$f = \frac{1}{T} = \frac{I_S}{C_0 \Delta V}, \tag{3}$$

where C_0 and ΔV are constant, and ΔV is limited by V_{TOP} and V_{REF}.

$$\Delta V = V_{TOP} - V_{REF}. \tag{4}$$

Obviously, f is proportional to the redox current I_S and we can easily estimate the redox current through the frequency of the periodic signal. C_0 should be chosen carefully, if C_0 is too large, a long time is needed to charge and discharge C_0; but if C_0 is too small, the resolution could be affected by a leakage current and parasitic effects. The capacitance value of C_0 chosen in this design is 100 fF, and the work frequency of the sawtooth oscillator ranges from 10 Hz to 10 MHz. C_1 and C_2 are used to control the recharging time, if C_1 and C_2 are very small, the recharging time is too short to charge C_0 to V_{TOP}; however, if C_1 and C_2 are very large, the chip size increases and the resolution of the system is reduced. C_1 and C_2 can be obtained through EDA simulation.

3.3. Digital frequency meter

The digital frequency meter is used to detect the frequency of the periodic pulse generated by the sawtooth oscillator, and further delivers to a 10-bit digital output. A detailed schematic of the digital frequency meter is shown in Fig. 3.

The digital frequency meter is composed of two binary asynchronous counters and control logic. Counter 1 and

counter 2 count the cycles of the clock and of V_C, respectively. The operation of the two counters is controlled by the control logic. Counter 1 starts to count the cycles of the clock after a reset, and counter 2 starts to count the cycles of V_C when counter 1 reaches five (0101), and the two counters stop counting when counter 1 reaches ten (1010). According to the circuit, five cycles of the reference clock cover the same time span as S (output of counter 2) cycles of V_C; so the frequency of the sawtooth wave f is given by

$$f = \frac{f_{CLK}}{5} S, \tag{5}$$

where f_{CLK} is the frequency of the reference clock. From Eqs. (3) and (5),

$$I_S = \frac{f_{CLK} C_0 \Delta V}{5} S. \tag{6}$$

From Eq. (6), the redox current (I_S) is evidently proportional to the output number of counter 2 (S).

4. Nonideality analysis and design optimization

The main nonideality characteristics that affect the measurement resolution and linearity of the system include input noise, leakage current, recharging time of C_0, and the measurement error of the digital frequency meter. We have analyzed these nonideality characteristics in this paper and optimized the design to keep the impact on the measurement accuracy as low as possible. Moreover, we reduce the measurement error of I_S through calibration, and reduce the measurement error of the digital frequency by adjusting the reference clock.

4.1. Input referred noise

The operation transconductance amplifier (OTA) used in this design is shown in Fig. 6. In a potentiostat, the potential variation on the work electrode is due to the finite gain and the input referred noise. So the OTA with a large DC gain (over 75 dB in the design) is preferred to reduce the potential variation. The noise potential power spectral density, $\overline{V_{n,tot}^2}$, in a single transistor is given by

$$\overline{V_{n,tot}^2} = \frac{4kT\gamma}{g_m} + \frac{K}{C_{ox} W L f}. \tag{7}$$

An analysis of the OTA reveals that the noise contributed by M0 and M5–M8 can be neglected; the total noise is mainly contributed by M1–M4, M9, and M10. The input referred noise of OTA is given by

$$\overline{V_{n,tot}^2} = \frac{8kT\gamma}{g_{m1,2}} \left(1 + \frac{g_{m3,4}}{g_{m1,2}} + \frac{g_{m9,10}}{g_{m1,2}}\right) + \frac{2K_N}{C_{ox} W_{1,2} L_{1,2} f} + \frac{2K_N}{C_{ox} W_{3,4} L_{3,4} f} \frac{g_{m3,4}^2}{g_{m1,2}^2} + \frac{2K_P}{C_{ox} W_{3,4} L_{3,4} f} \frac{g_{m9,10}^2}{g_{m1,2}^2}. \tag{8}$$

We have increased W/L and the drain current of M1 and M2 to increase $g_{m1,2}$, and sized other devices such that $g_{m3,4}$ and $g_{m9,10} \ll g_{m1,2}$ to minimize the noise contributions of devices M3, M4, M9, and M10. Moreover, all transistors should be sized as large as possible to minimize the $1/f$ noise.

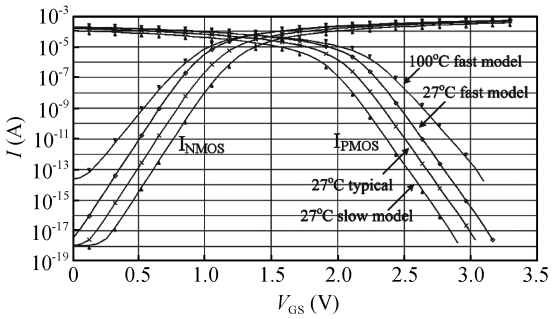

Fig. 7. Corner analysis simulated I_{DS} versus V_{GS}.

4.2. Leakage current

The smallest MOS transistor current is limited by its leakage current. However, in modern CMOS process, because of the ion implantation for lowering the threshold voltage, the effective leakage current (for $V_{GS} = 0$) of a minimum size MOS transistor may be as large as 10 pA[20]. Obviously, this cannot satisfy the requirements of this design. We can reduce the leakage current to the level of diffusion reverse leakage currents by either biasing the gate voltages beyond the power supply rails or by slightly shifting the source voltages[20]. Through simulation and corner analysis in Spectre, the leakage current of a MOS transistor can be reduced to approach the diffusion reverse leakage current by shifting the source voltage up or down by 400 mV. Even in the worst case, i.e., a fast MOS model and 100 °C, the leakage current is below 10^{-14}A. The simulation result is shown in Fig. 7. In our design shown in Fig. 3, V_{TOP} should be decreased at least 400 mV below V_{dd} to guarantee that the leakage current is much smaller than the measured redox current.

4.3. Calibration

From Eqs. (2) and (3), we can derive the sensing current I_S. T in Eqs. (2) and (3) represents the period of the periodic pulse, neglecting the recharging time of C_0. Due to parasitic capacitances and manufacturing variations, the real value of the charging and discharging capacitor C_0 in every single chip is different from its design value. Fortunately, we can eliminate these effects through calibration. Assuming the total capacitance value between the terminal Z and ground is C_{tot} and taking into account the propagation delay time t_P, Equations (2) and (3) can be rewritten as

$$\frac{1}{f} - t_P = \frac{C_{tot} \Delta V}{I_S}. \tag{9}$$

Because the propagation delay time t_P limited by the control block shown in Fig. 3 is invariable, we can figure out t_P by measuring the system with two reference currents (I_{S1}, f_1, I_{S2}, f_2).

$$\frac{1}{f_1} - t_P = \frac{C_{tot} \Delta V}{I_{S1}}, \tag{10}$$

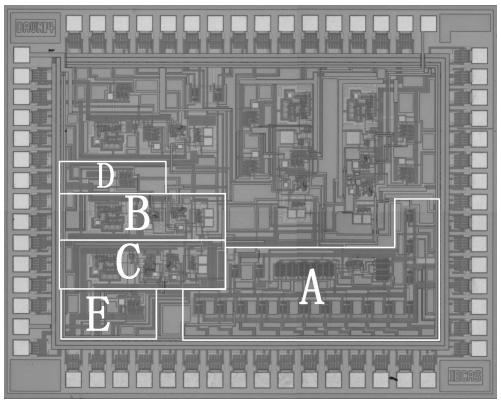

Fig. 8. Photograph of the prototype chip (2×2.5 mm^2). The sub blocks are (A) digital frequency meter, (B) the potentiostat, (C) the low current sawtooth oscillator, (D) the analog buffer, and (E) the digital buffer.

$$\frac{1}{f_2} - t_{\mathrm{P}} = \frac{C_{\mathrm{tot}}\Delta V}{I_{\mathrm{S2}}}. \tag{11}$$

From Eqs. (10) and (11), we can derive

$$C_{\mathrm{tot}}\Delta V = \frac{(1/f_1 - 1/f_2)I_{\mathrm{S1}}I_{\mathrm{S2}}}{I_{\mathrm{S2}} - I_{\mathrm{S1}}}, \tag{12}$$

$$t_{\mathrm{P}} = \frac{I_{\mathrm{S2}}/f_2 - I_{\mathrm{S1}}/f_1}{I_{\mathrm{S2}} - I_{\mathrm{S1}}}. \tag{13}$$

After calibration, we can obtain a more precise current I_{S} from Eq. (9).

4.4. Nonlinearity and error analysis

We neglect the charging time of C_0 in Eq. (2), but in fact, the redox current is proportional to the discharging time of C_0, so the charging time of C_0 brings nonlinearity to the sawtooth oscillator. The linearity of the sawtooth oscillator becomes worse when I_{S} becomes larger. We can reduce the nonlinearity through calibration, as mentioned in Section 4.3.

Due to the asynchrony between the clock and V_{C}, the digital frequency meter is accompanied by a measurement error during frequency testing. Because the counters just count integral cycles, the maximum error is 1 LSB of counter 2: that is, one cycle of V_{C}. In order to reduce the measurement error, we can adjust the frequency of the clock during testing to make sure that the frequency of the clock is much smaller than the frequency of V_{C}. Moreover, we can increase the output bits of the system to satisfy the requirements of wide dynamic range and high precision, but this happens at the cost of chip size, power dissipation, and speed. Note that when the redox current is very small, it will take a long time to measure the current. We could reduce the measurement time by decreasing ΔV.

5. Experiment results

The prototype chip was fabricated in a standard 0.35 μm, 2-poly and 4-metal layer CMOS process (Chartered Semiconductor). The whole chip size is 2×2.5 mm^2, and the die size of the readout circuit is approximately 680×1800 μm^2. The circuit is designed for a supply voltage of 3.3 V. Figure 8 shows a photograph of the whole prototype chip, where a full custom layout has been employed.

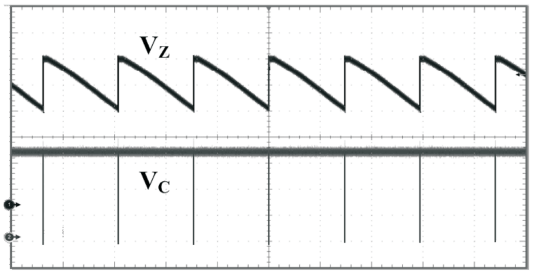

Fig. 9. Test waveform of the sawtooth oscillator.

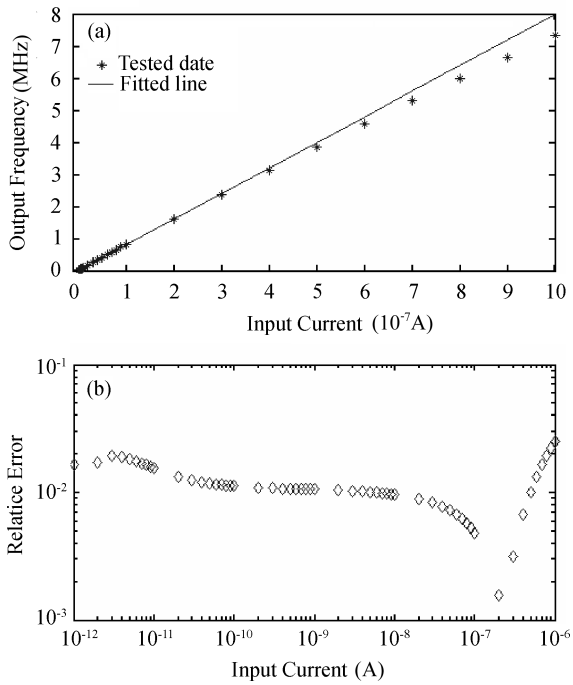

Fig. 10. Measured frequency and relative error versus input current.

Table 2. Summary of the interface chip specifications.

Parameter	Specification
Technology	0.35 μm 2P4M CMOS
Power supply	3.3 V
Measurement accuracy	10 bits
Current measurement range	1 pA–300 nA
Maximum non-linearity	0.3%
Chip size	2×2.5 mm^2

The performance of the weak current readout circuit has been verified with specially designed current sources. Currents from 1 pA to several hundred nanoamperes can be obtained from the current source. Output currents with low noise from the source are quite stable and can serve as a substitute for the redox current of the sensor. Figure 9 shows the tested waveforms of V_{Z} and V_{C} with a 7 pA input reference current, and the tested frequency of the sawtooth waveform is 61.3 Hz.

The measured results are plotted in Fig. 10. Figure 10(a) shows the output frequency versus the input current in linear coordinates, and Figure 10(b) plots the tested relative error versus the different input currents in logarithmic coordinates.

Table 3. Comparison with reported results.

Parameter	Lowest current (pA)	Dynamic range (dB)	Power (mW)	Resolution	Process (μm)	Supply voltage (V)
Bandyopadhyay[8]	500	120	0.5	250 pA	0.5	5
Akerow[9]	100	75	NA	100 pA	1	5
Turner[11]	0.10	32	2	10 nA	5	NA
Narula[14]	1	106	0.13	100 fA	0.5	5
Breten[17]	> 10	74	NA	11 bits	0.7	5
This work	1	110	1.49	10 bits	0.35	3.3

The test results gradually deviate from the fitted line with input currents over 300 nA. Generally speaking, the readout circuit functions well. The circuit has good linearity over the range from 1 pA to 300 nA, and its relative error is less than 0.02 over the full scale.

After calculation and calibration, we can figure out the measured current. Currents from 1 pA to 300 nA can be detected with a maximum nonlinearity of 0.3%. The characteristics of this chip are summarized in Table 2. A comparison of our test results with earlier reported results is summarized in Table 3.

6. Conclusion

A fully integrated CMOS weak current readout circuit is demonstrated. This design converts the input current directly into a periodic pulse signal, which can be conveniently processed by the successive digital circuit. The readout circuit consists of a fast stabilization enhanced potentiostat, a low current controlled sawtooth oscillator and a digital frequency meter. The design of these blocks has been discussed, together with the optimization of the circuit and system.

The chip was fabricated in a chartered 0.35 μm standard CMOS process. Measurements on the circuit have been performed and the feasibility of the readout structure has been proven. Currents from 1 pA to 300 nA can be detected with a maximum nonlinearity error of 0.3%. The interface circuit achieves more than a 100 dB dynamic range and a 10 bits measured resolution, which should meet the specifications required by amperometric micro-sensors.

References

[1] Zhang Lei, Gu Zhen, Yu Zhiping, et al. A CMOS microarray with on-chip decoder/amplifier and its integration with a bio-nano-system. Journal of Semiconductors, 2008, 29(10): 1947

[2] Yershov G, Barsky V, BeGovskiy A, et al. DNA analysis and diagnostics on oligonucleotide microchips. Proc Natl Acad Sci USA, 1996, 93: 4913

[3] Ekanayake E M I, Preethichandra D M G, Kaneto K. An amperometric glucose biosensor with enhanced measurement stability and sensitivity using an artificially porous conducting polymer. IEEE Trans Instrumentation and Measurement, 2008, 57(8): 1621

[4] Chung W Y, Paglinawan A C, Wang Y H, et al. A 600 μm readout circuit with potentiostat for amperometric chemical sensors and glucose meter applications. IEEE Electron Devices and Solid-State Circuits, 2007: 1087

[5] Huang C Y, Wang Y C, Chen H C, et al. Design of a portable potentiostat for electrochemical sensors. IEEE ISSNIP, 2004

[6] Li C, Yang H G, Xia S H, et al. Modeling of amperometric immunosensor for CMOS integration. Rare Metal Materials and Engineering, Jan 2006, 35: 439

[7] Steyaert M, Sansen W, Zhongyuan C. A micropower low-noise monolithic instrumentation amplifier for medical purposes. IEEE J Solid-State Circuits, 1987, 22(8): 1163

[8] Bandyopadhyay A, Mulliken G, Cauwenberghs G, et al. VLSI potentiostat array for distributed electrochemical neural recording. Proc IEEE Int Symp Circuits and Systems, 2002, II: 740

[9] Frey A, Jenkner M, Jenkner M, et al. Design of an integrated potentiostat circuit for CMOS bio sensor chips. Proc IEEE Int Symp Circuits and Systems, 2003, 5: 9

[10] Kakerow R, Kappert H, Spiegel E, et al. Low-power single chip CMOS potentiostat. Proc Solid-State Sensors and Actuators, 1995, 1: 142

[11] Tuner R, Harrison D, Baltes H. A CMOS potentiostat for amperometric chemical sensors. IEEE J Solid-State Circuits, 1987, 22(3): 473

[12] Martin S M, Gebara F H, Strong T D, et al. A low-voltage, chemical sensor interface for systems-on-chip: the fully differential potentiastat. Proceeding of IEEE International Symposium on Circuits and Systems, 2004, 4: 892

[13] Bian C, Xia S, Xu Y, et al. A micro amperometric immunosensor based on two electrochemical layers for immobilizing antibody. The 4th IEEE Conference on Sensors Proceedings, 2005: 416

[14] Narula H, Harris J. A time-based VLSI potentiostat for ion current measurements. IEEE Sensors Journal, 2006, 6(2): 239

[15] Narula H, Harris J. VLSI potentiostat for amperometric measurements for electrolytic reactions. IEEE ISCAS, 2004: 457

[16] Turner R, Harrison J, Baltes H. A CMOS potentiostat for amperometric chemical sensors. IEEE J Solid-State Circuits, 1987, sc-22(3): 473

[17] Breten M, Lehmann T, Bruun E. Integrating data converters for microampere currents from electrochemical transducers. IEEE International Symposium on Circuits and Systems, 2000: 709

[18] Hasan S M R. Stability analysis and novel compensation of a CMOS current-feedback potentiostat circuit for electrochemical sensors. IEEE Sensors Journal, 2007, 7(5): 814

[19] Razavi B. Design of analog CMOS and integrated circuits. The McGraw-Hill, 2003: 240

[20] Linares-Barranco B, Serrano-Gotarredona T. On the design and characterization of femtoampere current-mode circuits. IEEE J Solid-State Circuits, 2003, 38(8): 1353